Int. J. Solids Structures, 1976, Vol. 12, pp. 401–417. Pergamon Press. Printed in Great Britain.

ELASTIC STABILITY OF LAMINATED ELASTOMERIC COLUMNS

R. A. SCHAPERY
Departments of Aerospace and Civil Engineering, Texas A and M University, College Station, TX 77843, U.S.A.

and

D. P. SKALA
Lord Kinematics, 1635 W. 12th St., Erie, PA 16512, U.S.A.

(*Received* 27 *May* 1975; *revised* 29 *September* 1975)

Abstract—The effect of axial load on the behavior of columns consisting of alternate layers of rubber and curved or flat rigid shims is analyzed. First, finite difference equations governing the column response are derived. Relative movement between adjacent shims is assumed to be linear with respect to shearing force and bending moment, but the relation between axial load and this movement is not required to be linear. The equations are then approximated by letting the number of layers become infinite while the column length remains finite. The resulting differential equations for this so-called continuum column are solved for critical loads and mode shapes for globally homogeneous columns with three different end conditions. A general discrete analysis of the same problem, which is more appropriate for columns with a small number of layers and for nonhomogeneous columns, is also presented. Comparison of the two analyses establishes the limits of applicability of the approximate continuum analysis. The theory is then shown to agree quite well with experimental results for critical loads and mode shapes.

INTRODUCTION

A thin layer of rubber bonded between stiff reinforcements is capable of withstanding high compressive loads with only a small amount of normal deflection while, at the same time, offering little resistance to shearing[1]. Such *composite elements*, used singly or in stacks, have been widely employed as anti-vibration mounts, shock absorbers, and bridge bearing pads. In two relatively new applications, stacks of spherically-shaped elements consisting of steel reinforcements and rubber are being used as helicopter main rotor bearings and as supports for omniaxial movable rocket nozzles.

Although these stacks or so-called laminated bearings are usually quite stubby, instability under tensile and compressive axial loads can occur as a result of the low shearing resistance. An analytical understanding of their stability, therefore, is essential to the design process.

Several years ago, Gent[2] reported the results of an experimental and theoretical study on the behavior of columns composed of *flat* elements. He compared predictions from an approximate theory developed by Haringx[3–5] to compressive buckling loads and lateral deflections measured in a series of experiments on columns having three to twenty-three elements. Satisfactory agreement between theory and experiment was found in many cases. However, the measured buckling loads for columns with only a few elements were consistently above the predictions. This discrepancy is believed due, at least in part, to the fact that Haringx's analysis is for solid rubber rods, not for columns consisting of discrete units.

In this paper, we derive exact linear equations for predicting compressive and tensile instabilities. These equations take into account the composite structure of laminated columns; they are developed for flat and curved layers. In addition, a limiting form of these equations is deduced for the case of a finite-length column having an infinitely large number of layers. We then give some explicit analytical solutions for critical loads and associated mode shapes. As a matter of terminology, a column composed entirely of identical elements will be termed *homogeneous*, even though each element consists of rubber and stiff reinforcements. A finite-length column with an infinite number of elements will be called a *continuum column.*

We then consider the prediction of critical loads and mode shapes for both nonhomogeneous and homogeneous columns having a finite number of elements, using the original difference equations. The limits of applicability of the continuum-column analysis are investigated, and experimental confirmation of both the discrete and continuum analysis is presented.

DEVELOPMENT OF GOVERNING EQUATIONS

Notation for the column and a generic composite element is shown in Figs. 1 and 2. The column's centerline is, by definition, made up of straight line segments whose end points are in the exact center of each reinforcement or *shim*. A *composite element* is defined to consist of one rubber† layer plus one-half of the total shim thickness on each side of the rubber.

In the unloaded state, we assume that the column's centerline is straight and that the composite elements are symmetric with respect to imaginary planes which are perpendicular and parallel to the plane of the page and contain the column's centerline. The reinforcements are assumed to be perfectly rigid and, under load, to *not* suffer any displacement perpendicular to the plane of the page.

No other restrictions are placed on the column and element geometry. Therefore, the shims and rubber layers can be curved and can have non-uniform thicknesses. Also, there may be an axial

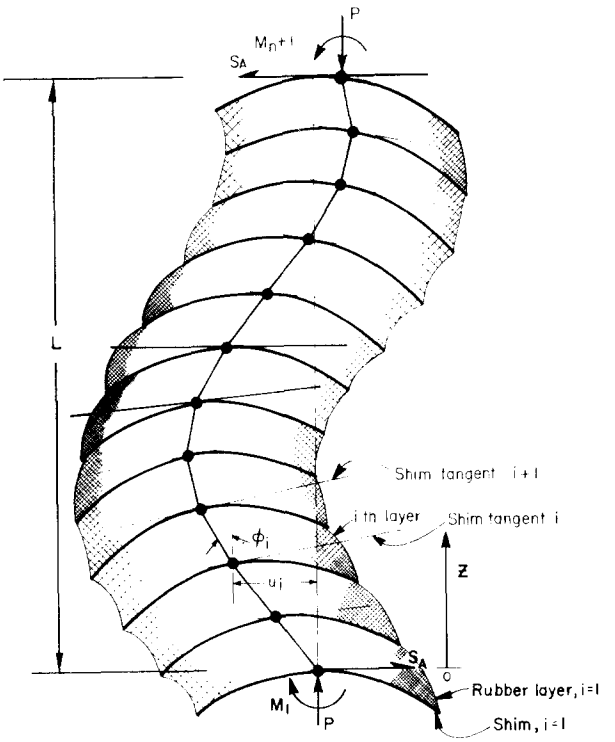

Fig. 1. Schematic diagram of laminated column.

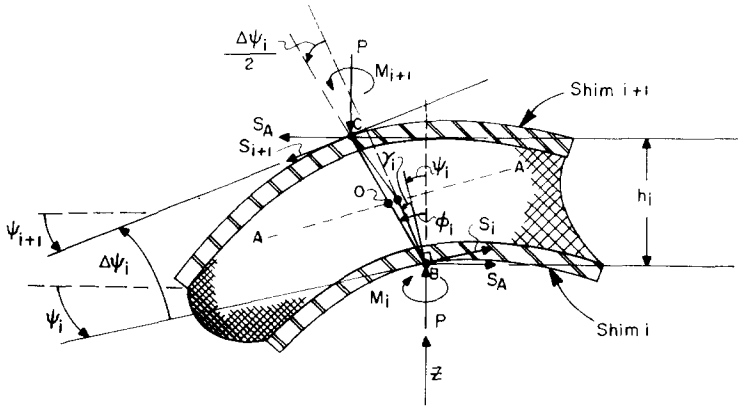

Fig. 2. Free body diagram of the ith composite element.

†The central material in the composite layer need not be rubber, but it must be soft relative to the shim material to satisfy the underlying assumption. The term "rubber" is intended to connote this compliance.

hole through the center of the column, and the material and geometric properties of the composite elements may vary along the column. For clarity, we have shown the elements as circular in cross-section in the figures, but they need not be so simple in shape nor even be smooth.

We shall assume that each composite element, when under axial load (tension or compression), is *linearly elastic* with respect to incremental bending and shearing deflections of the rigid shims. However, nonlinearities *are* allowed to the extent that the axial, bending, and shear stiffnesses of each composite block may depend on axial load; also, the change in column length due to axial load is *not* restricted to be small. Since the main objective of the analysis is to predict critical loads and mode shapes, and not post-buckling behavior, all angles which serve in defining changes in location and orientation of the shims are assumed to be small.

Referring to Fig. 2, the orientation of the ith shim is defined by the angle ψ_i between the tangent plane at point B (which is at the exact center of this shim) and the horizontal direction; for a flat shim this tangent corresponds, of course, to its entire center plane. An additional reference plane that will be used in the development is given by A–A in Fig. 2; this plane is *not* attached to a point on the rubber, but rather is exactly midway between the tangent planes at B and C.

Equilibrium equations

The axial load P is considered to be positive for compression and negative for tension. Also, the transverse shear load S_A and moments M_i and M_{i+1} are taken to be positive when they act in the directions shown in Fig. 2. With this convention, the summation of moments about point B in Fig. 2 yields

$$\Delta M_i = -S_A h_i - P h_i \phi_i, \tag{1}$$

where

$$\Delta M_i \equiv M_{i+1} - M_i, \tag{2}$$

and h_i is the length of centerline segment B–C when the column is under axial load.

Also of interest are the resultant moment $\bar{M}_i$ and shear force $\bar{S}_i$ acting at "0" on the imaginary plane A–A, which represent the reactions of the portion of the composite element below A–A on the portion above A–A; these quantities will prove to be useful in the constitutive equations for the element. Summing moments about "0" for the upper portion of the element and using (1) and (2), we find $\bar{M}_i$ is the average of the moments acting on adjacent tangent planes:

$$\bar{M}_i = (M_i + M_{i+1})/2 = M_i + \Delta M_i/2. \tag{3}$$

The orientation of A–A is defined by the angle

$$\bar{\psi}_i \equiv (\psi_i + \psi_{i+1})/2 = \psi_i + \Delta\psi_i/2, \tag{4}$$

using the definition

$$\Delta\psi_i \equiv \psi_{i+1} - \psi_i. \tag{5}$$

The shear force on A–A is then

$$\bar{S}_i = S_A + P\left(\psi_i + \frac{\Delta\psi_i}{2}\right) = S_A + P\bar{\psi}_i. \tag{6}$$

Inasmuch as the shear force on the ith tangent plane is $S_i = S_A + P\psi_i$, (4) and (6) yield

$$\bar{S}_i = (S_i + S_{i+1})/2, \tag{7}$$

and therefore $\bar{S}_i$ is the average of the shear forces on adjacent tangent planes.

In deriving the preceding equations, it was assumed that no external forces or moments are applied to the composite elements other than those at the ends of the column. However, the equations can be easily modified to account for loading on intermediate elements when it is desired

to investigate more general beam-column behavior. Also, by segmenting the column, the present equations will apply in the presence of certain types of additional external loads; for example, a column subjected to a central transverse shear load would be analyzed in the usual way by analyzing top and bottom halves separately and then applying matching conditions at the center.

Constitutive equations for the composite element

The total relative motion between two adjacent shims can be decomposed into relative axial displacement, $h - h_0$, pure bending, $\Delta\psi$, and simple shearing, γ, which are shown in Figs. 3–5,

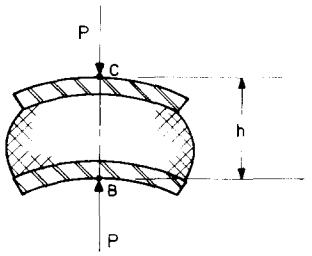

Fig. 3. Composite element with axial displacement.

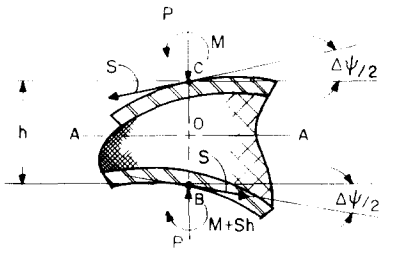

Fig. 4. Composite element with pure bending and axial displacement.

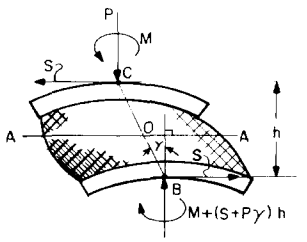

Fig. 5. Composite element with simple shearing and axial displacement.

respectively; h_0 is the unloaded composite element height. In this subsection we treat the three generalized displacements ϵ, $\Delta\psi$, and γ as independent variables, where

$$\epsilon \equiv (h_0 - h)/h_0, \tag{8}$$

which is obviously positive when the axial force is compressive. The generalized forces $\bar{M}$, $\bar{S}$, and P are the dependent variables.

Development of constitutive equations for the composite element is aided by making use of its strain energy function, U; for isothermal processes this function is the Helmholtz free energy and for adiabatic processes it is the internal energy [6]. First, it is necessary to determine the expression for virtual work, δW, done by the applied loads and moments when the independent variables $\Delta\psi$, γ, and ϵ undergo virtual changes $\delta(\Delta\psi)$, $\delta\gamma$, and $\delta\epsilon$.

Let us consider the ith composite element in Fig. 2, for which the relative position of the shims is given by $\Delta\psi_i$, γ_i and ϵ_i. Without loss in generality in the virtual work calculation, we can for simplicity consider the plane A–A to be fixed in space; there results,

$$\delta W_i = \bar{M}_i \delta(\Delta\psi_i) + h_i \bar{S}_i \delta\gamma_i + h_{0i} P \delta\epsilon_i. \tag{9}$$

Also, $U_i = U_i(\Delta\psi_i, \gamma_i, \epsilon_i)$, and therefore

$$\delta U_i = \frac{\partial U_i}{\partial \Delta\psi_i}\delta(\Delta\psi_i) + \frac{\partial U_i}{\partial \gamma_i}\delta\gamma_i + \frac{\partial U_i}{\partial \epsilon_i}\delta\epsilon_i. \tag{10}$$

Since $\delta U_i = \delta W_i$ for arbitrary virtual changes in $\Delta\psi_i$, γ_i, and ϵ_i, (9) and (10) yield

$$\bar{M}_i = \partial U_i/\partial \Delta\psi_i, \quad h_i \bar{S}_i = \partial U_i/\partial\gamma_i, \quad h_{oi} P = \partial U_i/\partial\epsilon_i. \tag{11}$$

For sufficiently small values of $\Delta\psi_i$ and γ_i, the change in strain energy may be approximated by the quadratic function

$$U_i(\Delta\psi_i, \gamma_i, \epsilon_i) - U_i(0, 0, \epsilon_i) = \frac{K_B{}^i}{2h_i}(\Delta\psi_i)^2 + K^i_{12}\Delta\psi_i\gamma_i + \frac{h_i K_S{}^i}{2}\gamma_i^2, \tag{12}$$

where the height, h_i, has been introduced for later convenience and

$$K_B{}^i \equiv h_i \frac{\partial^2 U_i}{\partial \Delta\psi_i^2}(0, 0, \epsilon_i), \tag{13a}$$

$$K_S{}^i \equiv \frac{1}{h_i}\frac{\partial^2 U_i}{\partial \gamma_i^2}(0, 0, \epsilon_i), \tag{13b}$$

$$K^i_{12} \equiv \frac{\partial^2 U_i}{\partial \Delta\psi_i \partial \gamma_i}(0, 0, \epsilon_i). \tag{13c}$$

We have used the fact that $\bar{M}_i = \bar{S}_i = 0$ when $\Delta\psi_i = \gamma_i = 0$ (regardless of the magnitude of ϵ_i) on account of the element's assumed symmetry about line CB.

The constitutive equations of the composite element for forces and moment are obtained by substituting (12) into (11):

$$\bar{M}_i = \frac{K_B{}^i}{h_i}\Delta\psi_i + K^i_{12}\gamma_i, \tag{14a}$$

$$\bar{S}_i = \frac{K^i_{12}}{h_i}\Delta\psi_i + K_S{}^i\gamma_i, \tag{14b}$$

$$P = \frac{1}{h_{oi}}\frac{\partial U_i}{\partial \epsilon_i}(0, 0, \epsilon_i), \tag{15}$$

where terms of second order in $\Delta\psi_i$ and γ_i have been neglected in (15). The coefficients $K_B{}^i$, $K_S{}^i$, and K^i_{12} will be called "bending stiffness", "shear stiffness", and "cross stiffness", respectively; it is to be noted that they may depend on the axial strain, ϵ_i.

These constitutive equations of the composite element serve to completely describe its macroscopic behavior. Note that all the variable information in these equations is available at points C and B; the constitutive equations serve only to describe the transmission of forces and moments between points C and B in terms of their relative displacement. The detailed way in which this is done is contained in the layer stiffnesses K_B, K_S, and K_{12}, and is immaterial to the buckling analysis itself. Relations (14) and (15) apply to elements with flat or curved shims. However, when the shims in a composite element are flat and have the same thickness, some simplification is possible as a result of geometric symmetry with respect to the plane A–A. Namely, referring to Fig. 4 in which $\gamma = 0$ and $\Delta\psi \neq 0$, it is clear that the shear stress along A–A in a flat rubber layer is zero. Hence, $\bar{S}_i = 0$, and (14b) yields $K^i_{12} = 0$. (It is of interest to observe that with the simple shearing case shown in Fig. 5, a moment has to be applied to the shims since $\bar{M} = 0$ implies $M = -h(P\gamma + S)/2$.)

Thus, for flat shims of equal thickness,

$$\bar{M}_i = \frac{K_B{}^i}{h_i}\Delta\psi_i, \tag{16a}$$

$$\bar{S}_i = K_S{}^i\gamma_i. \tag{16b}$$

With this result, we can identify our stiffnesses directly with the stiffnesses T' and K' used by Gent[2];

viz., $$T' = K_B, \quad K' = K_S. \tag{17}$$

Additional information on the stiffnesses in (14) is obtained by assuming the *composite element* is

stable in the neighborhood of $\Delta\psi = \gamma = 0$. This stability implies the change in strain energy, (12), is positive whenever $\Delta\psi$ and γ are not both zero; necessary and sufficient conditions for the existence of this behavior of the strain energy are

$$K_B^i > 0, \quad K_S^i > 0, \quad K_B^i K_S^i - (K_{12}^i)^2 > 0. \tag{18}$$

Although the bending and shear stiffnesses are positive, the cross stiffness may be negative. In fact, the sign of K_{12}^i is determined by the geometry of the shims relative to the positive direction of the z axis. For instance, if the elements are V-shaped and pointing upward, or are curved and concave downward, as in Fig. 5, then $K_{12}^i < 0$; this result can be inferred from (14a) after setting $\Delta\psi_i = 0$, $\gamma_i > 0$, and considering the nature of the stress distribution in the rubber.

Continuity equation for the column centerline

One further basic equation needed to analyze column stability relates the orientation of plane A–A, $\bar{\psi}_i$, shear angle γ_i, and angle between the column centerline and vertical axis ϕ_i. From Figs. 2 and 5, one finds $\phi_i = \bar{\psi}_i + \gamma_i$, and therefore

$$\phi_i = \psi_i + \frac{\Delta\psi_i}{2} + \gamma_i. \tag{19}$$

The complete set of equations governing column behavior, apart from specified boundary conditions, are (1), (6), (14) and (19), as well as the relations

$$\Delta G_i \equiv G_{i+1} - G_i, \tag{20a}$$

$$\bar{G}_i \equiv (G_{i+1} + G_i)/2, \tag{20b}$$

where G_i represents any generalized force or displacement associated with element i or node point i. Equation (15), which relates axial load and change in element height, is not needed *unless* there is an appreciable change in column length due to the load.

ANALYSIS OF CONTINUUM COLUMNS

When a column is made up of a large number of elements, we will approximate the above difference equations by differential equations. In so doing, we treat the deformed column centerline as a continuous curve, as opposed to a series of discrete straight line segments. Now consider this case—the continuum column—in order to gain insight into the stability behavior of laminated columns.

Governing equations

In the above-referenced equations, we let $h_i \to dz$ and $\Delta \to d$, drop the index "i", and obtain:

$$\frac{dM}{dz} = -S_A - P\phi, \tag{21}$$

$$S = S_A + P\psi, \tag{22}$$

$$M = K_B \frac{d\psi}{dz} + K_{12}\gamma, \tag{23}$$

$$S = K_{12} \frac{d\psi}{dz} + K_S\gamma, \tag{24}$$

$$\phi = \psi + \gamma. \tag{25}$$

Although these equations are valid for nonhomogeneous columns (i.e. the stiffnesses may be functions of z) we shall now assume all three stiffnesses are constant in z in order to simplify the analyses. Quite obviously, (23) and (24) could have been arrived at directly by a reasoning process similar to that used in the derivation of (9)–(14). The stiffnesses K_B, K_S, K_{12} in (23) and (24) have the

same physical meaning as those in (14a) and (14b), but here they refer to a point on the column axis rather than to a connection between two discrete points.

Equations (21)–(25) are first used to obtain

$$PK_{12}M - D\frac{dM}{dz} = (PK_B + D)(S_A + P\psi), \tag{26}$$

where

$$D \equiv K_B K_S - K_{12}^2. \tag{27}$$

Differentiation of (26) with respect to z and again using the above equations yields, finally,

$$\frac{d^2M}{dz^2} + q^2M = 0, \tag{28}$$

where

$$q^2 \equiv P(P + K_S)/D. \tag{29}$$

Notice that $D > 0$ for a stable composite element in view of (18). (It is of interest to point out that if the matrix of stiffnesses in (23) and (24) was not symmetric, a term proportional to dM/dz would have appeared in (28).)

The centerline deflection, $u = u(z)$, can be derived by using the relation (see Fig. 1)

$$\frac{du}{dz} = \phi, \tag{30}$$

and integrating (21). We find

$$u = u_1 - \frac{1}{P}(M - M_1) - \frac{S_A}{P}z, \tag{31}$$

where $M_1 \equiv M(0)$ and $u_1 \equiv u(0)$. The differential equation for displacement can be obtained by solving (31) for M and substituting the result into (28). When $M_1 = S_A = u_1 = 0$, it is seen that $u = -M/P$, and therefore the differential equation for u is identical to that for moment. (This latter equation for u, after setting $K_{12} = 0$, is the same one Haringx [3–5] derived for solid rubber columns using an approximate physical model, whose solutions were applied by Gent [2] to laminated columns with flat elements.) However, when these end values and shear force are not zero, the differential equation for u is not as simple as (28); for this reason, the moment will be used as the primary dependent variable in the remaining analysis.

When $q \neq 0$, the general solution to (28) is

$$M = A \cos qz + B \sin qz, \tag{32}$$

where q is the positive root of q^2, and A and B are constants. When $q = 0$,

$$M = A_1 z + B_1, \tag{33}$$

where A_1 and B_1 are constants. With reference to boundary conditions, it will be necessary to draw upon (26) and/or (31) unless both end moments are specified. Specifically, when the orientation of an end shim $\psi(0)$ and/or $\psi(L)$ is given, (26) provides the boundary condition needed in the solution for the moment distribution. Equation (31) is used if end displacement $u(0)$ is specified.

STABILITY ANALYSIS: PINNED-PINNED ENDS

The boundary or end conditions are $u(0) = u(L) = M(0) = M(L) = 0$, which when applied to solution (32), yield $A = 0$ and

$$qL = \pm\pi, \pm 3\pi, \ldots. \tag{34}$$

Substituting the smallest value of q^2L^2 into (29) we find the critical load to be

$$P = \frac{K_S}{2}[-1 \pm \sqrt{(1+\eta^2\pi^2)}], \tag{35}$$

where the (+) sign corresponds to a compressive ciritical load and the (−) sign to a tensile load. Also,

$$\eta \equiv \frac{2}{L}\sqrt{\left(\frac{K_B\lambda}{K_S}\right)}, \quad \lambda \equiv 1 - \frac{K_{12}^2}{K_B K_S}, \tag{36}$$

where $0 < \lambda \leq 1$ in view of (18); in the classical theory of columns $K_S^{-1} = K_{12} = 0$† and, therefore, $\eta = 0$ and $\lambda = 1$. The moment distribution associated with (35) is a half sine wave:

$$M = B \sin(\pi z/L), \tag{37}$$

where B is an indeterminate constant.

We must also determine if moment distribution (33) is applicable, as it may predict a smaller critical load than (35). The boundary conditions on moment yield $A_1 = B_1 = 0$; since $u(0) = u(L) = 0$, (31) yields $u = S_A = 0$. When these results are used together with (21)–(25) it is found that $\gamma = -\psi$, and

$$\psi(P + K_S\lambda) = 0. \tag{38}$$

A non-trivial solution, $\psi \neq 0$, can exist if a *tensile* load is applied with the value

$$P = -K_S\lambda, \tag{39}$$

where λ is given by (36).

Since $0 < \lambda \leq 1$, it follows from a comparison of (35) and (39) that the *tensile* critical load having the smallest magnitude is given by (39). The mode shape follows from (23) after setting $M = 0$ and $\gamma = -\psi$; the shim rotation is

$$\psi = \psi_0 e^{(K_{12}z/K_B)}, \tag{40}$$

where ψ_0 is the indeterminate rotation at $z = 0$.

Thus, when tensile load (39) is applied, the column remains straight but the shims rotate according to (40). If the shims are concave downward, as in Fig. 1, $K_{12} < 0$, and the shim rotation decreases exponentially from bottom to top; the orientations of the tangent planes are shown schematically in Fig. 6. For flat shims $K_{12} = 0$, and the orientation does not change along the length.‡ A simple physical explanation for tensile instability can be given for this latter case; viz., when $P < -K_S$, the shear force developed by the rubber as a result of the shear strain γ ($S = K_S\gamma = -K_S\psi$) is smaller in magnitude than the component of P in the tangent plane ($S = P\psi$).

STABILITY ANALYSIS: CLAMPED-CLAMPED ENDS

Substituting moment distribution (32) into (26) and (31), and invoking the end conditions $\psi(0) = \psi(L) = u(0) = u(L) = 0$, leads to a system of three homogeneous equations for the three constants A, B, and S_A. Requiring that the determinant vanish yields, after use of (29) and (36),

$$\sin x = g(y)\frac{2(1-\cos x)}{x}, \tag{41}$$

†In the classical treatment $\gamma = 0$, but S is non-zero, and an equation analogous to (16b) does not appear.

‡This case, as well as that of tensile buckling under clamped–clamped end conditions, has been observed experimentally. Unfortunately, these tests were performed well before the start of the present work and were not well-documented. The buckled column shapes, however, were recorded photographically, and agree qualitatively with the present predictions.

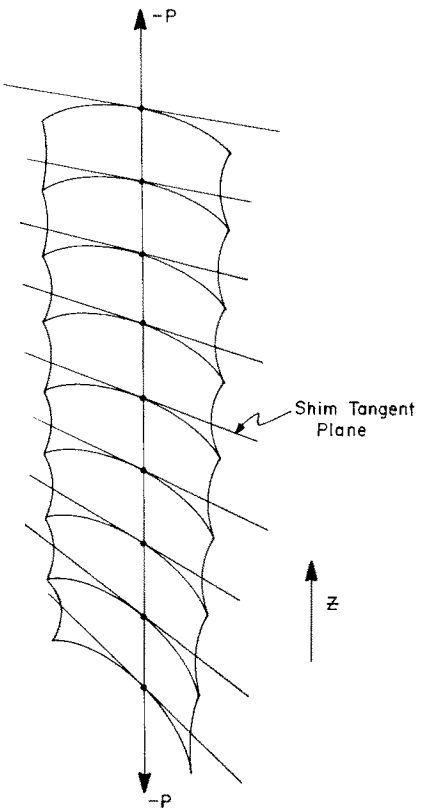

Fig. 6. Shim orientation for a column with pinned ends and $K_{12} < 0$ under the lowest critical tensile load.

where

$$x \equiv qL, \quad y \equiv \eta x, \tag{42}$$

and

$$g(y) \equiv \frac{y^2}{2[-1 \pm \sqrt{(1+y^2)}]}, \tag{43}$$

For a given value of η, (41) yields roots $x_1, x_2, \ldots$ which, in turn, enable the corresponding critical loads to be found from (29); explicitly,

$$P = \frac{K_S}{2}[-1 \pm \sqrt{(1+\eta^2 x^2)}], \tag{44}$$

where use of the (+) or (−) sign in (43) and (44) depends on whether P is compressive or tensile, respectively. Although (41) admits both negative and positive roots of equal magnitude, only the positive values need to be considered since x^2 rather than x appears in (44).

In contrast with the previous result for a column with pinned ends, we find that (33) leads only to the trivial result, $u = M = \psi = \gamma = 0$, regardless of the value or direction of the axial load. Therefore, the lowest tensile and compressive critical loads are to be obtained from (41)–(44). Investigation of the roots of (41) is aided by recognizing that when $P > 0$, $g(y)$ is a positive increasing monotonic function and $g(0) = 1$. When $P < 0$, $-g(y)$ is also a positive, increasing monotonic function in which $g(0) = 0$.

Figure 7 shows the left and right sides of (41), except for $g(y)$. For *compressive* loading, the above-mentioned behavior of g implies the first root is at $x = 2\pi$, regardless of the value of η. Therefore, the lowest critical load is

$$P = \frac{K_S}{2}[-1 + \sqrt{(1+4\eta^2\pi^2)}]. \tag{45}$$

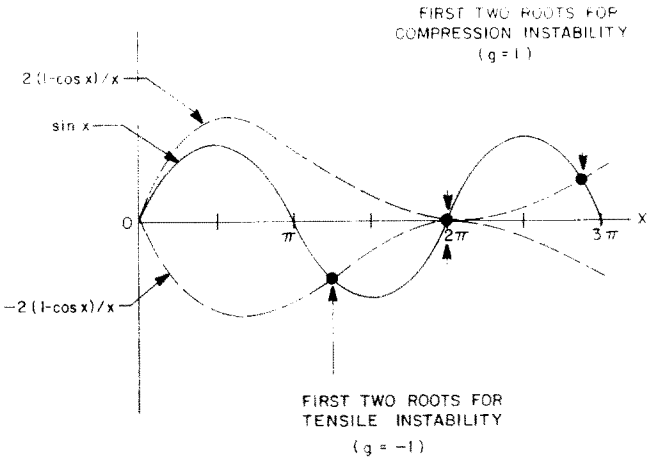

Fig. 7. Diagram illustrating the roots at eqn (41).

For this value, we find $B = S_A = 0$ and therefore

$$M = A \cos(2\pi z/L). \tag{46}$$

Referring again to Fig. 7, the first root for *tensile* instability is in the range $\pi < x < 2\pi$ whenever $\eta > 0$. This root increases monotonically from $x = \pi$ at $\eta = 0$, and $x \to 2\pi$ as $\eta \to \infty$. None of the constants A, B, S_A are zero for $\eta > 0$.

Inasmuch as $g \to \infty$ as $\eta \to \infty$ for compressive loading, (41) and Fig. 7 reveal that the second root, say x_2, approaches the first root, $x_1 = 2\pi$, as $\eta \to \infty$. A similar situation exists for tensile loading since $-g \to \infty$ as $\eta \to \infty$, and therefore the first root, x_1, approaches the second one, $x_2 = 2\pi$, as $\eta \to \infty$. The implication of this behavior is that the first and second critical loads approach one another for columns with high shape factors; i.e. for relatively low shear stiffness and/or small length, in view of definition (36) for η^2. (As an example, the ratio of second-to-first critical compressive load is 1·03 when $\eta = 10$.) When this closeness exists, minor imperfections in the column's construction or in its loading may cause both first and second modes to exist together. We have, in fact, observed deflections of this type under axial compression.

STABILITY ANALYSIS: CLAMPED-FREE ENDS

The end conditions are given as $M(0) = S_A = u(L) = \psi(L) = 0$. A non-trivial moment distribution (33), corresponding to $q = 0$, which satisfies these boundary conditions does not exist. Therefore, we concern ourselves only with solution (32); since $M(0) = 0$, $A = 0$ and therefore

$$M = B \sin qz. \tag{47}$$

Application of (26) to the end $z = L$ and use of the specified boundary conditions yields

$$\frac{\tan x}{x} = \frac{K_{12}}{|K_{12}|} \frac{\lambda}{1-\lambda} \frac{\eta}{[-1 \pm \sqrt{(1+\eta^2 x^2)}]}, \tag{48a}$$

where $|\ |$ denotes absolute value and, as before, the (+) is used when $P > 0$ and (−) when $P < 0$. The smallest root is found to be in different ranges depending on the sign of P and K_{12}. Specifically, a study of (48a) shows the following ranges of solutions.

$$\begin{array}{llll}
P>0, & K_{12}>0: & \eta \neq 0 & :0<x<\pi/2 \\
P>0, & K_{12}<0: & \eta \neq 0 & :\pi/2<x<\pi \\
P<0, & K_{12}>0: & \eta \neq 0 & :\pi/2<x<\pi \\
P<0, & K_{12}<0: & \eta \geqslant 2\sqrt{[(1-\lambda)/\lambda]} & :0 \leqslant x \leqslant \pi/2 \\
P<0, & K_{12}<0: & \eta < 2\sqrt{[(1-\lambda)/\lambda]} & :\pi<x<3\pi/2
\end{array} \tag{48b}$$

For flat shims, $K_{12} = 0$ and (48a) yields $x = \pi/2$ for tension and compression, regardless of the value of η. It is very interesting to note that when $K_{12} \neq 0$, the buckled column may be S-shaped instead of being a quarter-sine wave as in the classical theory of buckling. The critical load itself follows from (44) after substituting the appropriate root from (48a).

ANALYSIS OF THE DISCRETE NON-UNIFORM COLUMN

Let us return to the original governing equations for finite-sized elements in order to account for the true discrete nature of the column. We shall obtain explicit discrete solutions for critical loads and mode shapes, which provides a means of determining the range of validity of the continuum solutions. Most importantly, however, the discrete analysis enables us to easily analyze nonuniform columns, as the complexity of the continuum equations appears to preclude obtaining simple closed-form solutions for these columns.

We now use equations (1), (14), (19) and (20) directly to derive the governing difference equation of the column. The choice of an independent variable is again somewhat arbitrary; however, in correspondence with the continuum analysis we choose the moments M_k, $1 \leq k \leq n+1$. Eliminating all variables except the moments, we combine the governing equations to obtain the following:

$$\left\{b_{i-1} + \frac{(2+a_{i-1})(2-a_{i-1})}{h_{i-1}+d_{i-1}}\right\} M_{i-1} + \left\{b_i + b_{i-1} - \frac{(2+a_i)^2}{h_i+d_i} - \frac{(2-a_{i-1})^2}{h_{i-1}+d_{i-1}}\right\} M_i + \left\{b_i + \frac{(2+a_i)(2-a_i)}{h_i+d_i}\right\} M_{i+1} = 0, \quad 2 \leq i \leq n, \tag{49}$$

where the following definitions have been used:

$$a_i \equiv \frac{Ph_i K_{12}^i}{Q_i}, \tag{50}$$

$$b_i \equiv \frac{Ph_i K_S^{\,i}}{Q_i}, \tag{51}$$

$$d_i \equiv \frac{Ph_i K_B^{\,i}}{Q_i}, \tag{52}$$

$$Q_i \equiv K_B^{\,i} K_S^{\,i} - K_{12}^{i} > 0. \tag{53}$$

The moment equation for End No. 1 is

$$\left\{b_1 - \frac{(2+a_1)^2}{h_1+d_1}\right\} M_1 + \left\{b_1 + \frac{(2+a_1)(2-a_1)}{h_1+d_1}\right\} M_2 = -4\{S_A + P\psi_1\}, \tag{54}$$

and for the other end of the column,

$$\left\{b_n + \frac{(2+a_n)(2-a_n)}{h_n+d_n}\right\} M_n + \left\{b_n - \frac{(2-a_n)^2}{h_n+d_n}\right\} M_{n+1} = 4\{S_A + P\psi_{n+1}\}. \tag{55}$$

By summing (1) for $1 \leq i \leq n$, and noting that

$$\phi_i \equiv \frac{\Delta u_i}{h_i}, \tag{56}$$

we obtain the result

$$M_{n+1} - M_1 = -S_A L - PU, \tag{57}$$

where

$$L \equiv \sum_{i=1}^{n} h_i, \quad \text{the column height,} \tag{58}$$

and

$$U \equiv u_{n+1} - u_1, \tag{59}$$

the net transverse displacement across the column.

Equation (57) is nothing more than a requirement that the column as a whole remain in rotational equilibrium under the action of external moments and forces.

Two end conditions of interest are the pinned end and the clamped end. In both cases, the end condition $U = 0$ must also be used. We now have from (57)

$$S_A = \frac{1}{L}(M_1 - M_{n+1}). \tag{60}$$

The relevant boundary equations are as follows:

(a) Pinned ends: S_A and ψ unspecified and

$$M_1 = 0, \quad \text{(End 1)}, \tag{61a}$$

$$M_{n+1} = 0, \quad \text{(End } n+1\text{)}. \tag{61b}$$

(b) Clamped ends: S_A unspecified, and $\psi = 0$ yields

$$\left\{b_1 - \frac{(2+a_1)^2}{h_1+d_1} + \frac{4}{L}\right\} M_1 + \left\{b_1 + \frac{(2+a_1)(2-a_1)}{h_1+d_1}\right\} M_2 - \left\{\frac{4}{L}\right\} M_{n+1} = 0, \quad \text{(End 1)}, \tag{62a}$$

$$\left\{-\frac{4}{L}\right\} M_1 + \left\{b_n + \frac{(2+a_n)(2-a_n)}{h_n+d_n}\right\} M_n + \left\{b_n - \frac{(2-a_n)^2}{h_n+d_n} + \frac{4}{L}\right\} M_{n+1} = 0, \quad \text{(End } n+1\text{)}. \tag{62b}$$

Whenever the ends are either pinned or clamped, the boundary conditions (61) and (62) are homogeneous, and the entire system of moment equations can be represented by the homogeneous matrix equation

$$[A]\mathbf{M} = \mathbf{0}. \tag{63}$$

An examination of (49), (61) and (62) shows that the matrix $[A]$ is symmetric. Moreover, it is almost tridiagonal; in the clamped–clamped case, the upper right and lower left corner elements are nonzero. In the case of mixed or pinned–pinned end conditions $[A]$ is exactly triadiagonal. It is $(n+1)\times(n+1)$; $\mathbf{M}$ is an $(n+1)$ vector; $\mathbf{0}$ is the $(n+1)$ null vector.

We are concerned here with the situation where homogeneous end conditions are applied at the column ends and maintained while a *compressive* axial load P is quasistatically increased from zero. Although (63) represents a system of linear equations, almost all the elements of $[A]$ are nonlinear functions of P. For $0 \leq P < P_c$, the matrix $[A]$ will be nonsingular so that the only solution of (63) is the trivial one, $\mathbf{M} = \mathbf{0}$, implying that the column must remain straight for these values of axial load. However, at some critical load P_c the matrix $[A]$ will become singular. At $P = P_c$, besides the trivial solution, there exists a singly infinite family of solution vectors such that the column is capable of assuming a definite buckled shape (or theoretically of remaining straight). Although the mode shape corresponding to P_c is definite, the idealization of the column geometry and of its loading conditions preclude a calculation of its magnitude.

The real column, of course, differs from its mathematical idealization in that it has minor constructional defects. In addition, its loading conditions cannot be exactly ideal. The behavior of the real column is characterized by a rapid increase in transverse deformation as P approaches P_c. The type of column discussed here is capable of quite large deformations in general so that buckled columns may become violently distorted without rupturing. These extreme shapes cannot be predicted by the present analysis since they violate the small angle assumptions. In addition, the layer constitutive equations (14a) and (14b) are valid only for relatively small deformations. Nevertheless, the observed column shape at the onset of buckling is expected to correspond to the calculated one.

Higher order buckling modes exist but are of little practical interest. Although we have not

investigated these in any detail, the n layer column should have n compressive critical loads, the highest mode shape composed of alternating excursions of each shim.

Determining the compressive critical load is equivalent to finding that value of P (in particular, the smallest positive value) which causes $[A]$ to become singular. We have formulated an algorithm to do this which involves a direct calculation of the determinant of $[A]$ and its derivative with respect to P. Both these quantities are calculated in an iterative fashion. At each iterative step, both are scaled by the same arbitrary positive number to avoid numerical difficulties. The algorithm to calculate P_c uses the Newton–Raphson method to make det$[A]$ zero. This method uses only the ratio of the function to its derivative, which is independent of the arbitrary scaling used in the calculation of det[A]. The initial estimate of P_c is provided by the continuum analysis. It is the smallest of the buckling loads of a series of hypothetical uniform columns, each of the same height as the real column and having the same number of layers. These hypothetical columns are composed of identical layers, each column corresponding to an individual layer in the original column.

This algorithm was incorporated into a Fortran program which produced the numerical results which follow. The program calculates the critical load to one part in 10^6 and generates a diagram of the corresponding mode shape showing the displacement and orientation of the planes tangent to the shim center points. This diagram is arbitrarily scaled to a convenient value. The details of the numerical analysis procedure are given in [10].

ACCURACY OF THE CONTINUUM ANALYSIS

Having the discrete analysis, we are now in a position to evaluate the error involved in the continuum analysis of the uniform column. In general, the error will depend on the relative magnitudes of the three layer stiffnesses. In the case $K_{12} = 0$, however, we can estimate the error independent of the ratio K_B/K_S. To do this, we specialize (49) to the case of uniform, flat ($K_{12} = 0$) layers. After simplification, this reads

$$M_{i-1} - \rho M_i + M_{i+1} = 0, \tag{64}$$

where

$$\rho \equiv 2\left\{\frac{4-\beta}{4+\beta}\right\}, \tag{65}$$

and

$$\beta \equiv h^2 \frac{P}{K_B}\left(1+\frac{P}{K_S}\right). \tag{66}$$

From eqn (29) note that

$$\beta = h^2 q^2. \tag{67}$$

To compare the continuum with the discrete analysis, we calculate β_c, corresponding to P_c, using both analyses. For the continuum analysis, replace L by nh.

Table 1 shows the comparison between the two analyses for clamped–clamped end conditions for various values of n. Because of symmetry, the same values apply in both analyses to

Table 1. Buckling loads of continuum and discrete columns under clamped end conditions

$$\beta_c \equiv h^2 \frac{P_c}{K_B}\left(1+\frac{P_c}{K_S}\right)$$

No. layers	β_c (discrete)	β_c (continuum)	Error
2	∞	9·86	—
3	12·0	4·38	63·5%
4	4·0	2·46	38·5%
5	2·12	1·58	25·5%
6	1·33	1·10	17·3%
8	0·687	0·617	10·2%
10	0·422	0·395	6·4%

pinned–pinned columns having half as many layers. The tabulated percent error in β_c is actually larger than the error in P_c. Consequently, the use of the continuum analysis to calculate critical loads should be quite accurate providing there are at least 10 layers in a clamped column or 5 layers in a pinned column.

EXPERIMENTAL RESULTS

As a partial verification of both stability analyses, a series of five uniform laminated columns were built and tested. Each column was cylindrical in shape, 2·0″ outside diameter, and composed of thirty identical 0·100″ thick rubber disks, twenty-nine identical spherically curved stainless steel shims, and two end pieces of the same spherical radius as the shims. The elastomer was a medium stiffness natural rubber compound having a shear modulus† of 155 psi and a bulk modulus of 200,000 psi [9]. The columns were bonded into a unit using epoxy adhesive at 150°F. The shim spherical radius ranged from 1·55″ to ∞ (flat). Total column height varied from sample to sample due to varying shim curvature, thickness, and adhesive layer thickness. The layer thicknesses (1/2 shim + adhesive + rubber + adhesive + 1/2 shim) were assumed to be the same in any given sample and were inferred from the total column height and the known dimensions of the end pieces.

The columns were loaded on a screw operated universal testing machine at the rate of 0·04″/min until the load reached a maximum and started to fall off. Each column was tested several times. The buckled mode shapes were recorded photographically at their respective limit loads during the first and second loadings.

The buckling loads of the five columns were calculated using both the discrete and the continuum analysis. Agreement between the two analyses is better than 0·6% in all cases. The layer stiffnesses K_B, K_S and K_{12} were calculated as described in [7]. In these calculations, the shims were treated as perfectly rigid and the rubber as linearly elastic. The unloaded column length was used in all buckling predictions.

Table 2 shows a summary of the column data, as well as the predicted buckling loads and observed first cycle limit loads. Critical loads could not be determined experimentally (except perhaps in a very subjective fashion), since in general, the load-deflection curves were nonlinear along most of their length. Southwell's method [8] was not used since, except for Sample No. 1, the deformed columns were asymmetric. Some of the columns experienced a partial debonding between metal shim and elastomer which was visible in the photograph of the second test but not the first. For this reason, we restrict our attention to first cycle data. The observed first cycle limit loads are all high compared to the calculated critical loads, which is to be expected since these columns are capable of relatively large elastic deformations; some of this discrepancy is due to the use of the unloaded column length, rather than the length under critical load, and third-cycle shear modulus in the predictions. The onset of buckling was observed to be more gradual for the columns with more curved shims. The falloff of critical load with test cycle is believed due to slight changes in shear modulus (as reflected by the reduction in initial slope of the curves in Fig. 8) and to cumulative internal layer damage caused by the excessive deflections in the buckled configuration. We consider the agreement between theory and experiment shown in Table 2 to be adequate for design purposes.

The load-deflection data in Fig. 8 for Sample No. 3 is representative of all the data. Also shown is the calculated spring rate of the column, which is in excellent agreement with the experimental curve. Although the element compressive stiffness does not enter directly into the stability analysis, this good agreement is an indication of accuracy in the other calculated element stiffnesses [7]. Figure 9 shows a comparison of observed and calculated mode shapes for Sample No. 4. These are in good agreement. The calculated shapes were drawn by the computer to a fixed arbitrary scale. Sample No. 1 buckled into a symmetric shape as observed by Gent [2]. Samples No. 2–No. 5 were S-shaped, with the greatest departure from symmetry corresponding to the smallest spherical radius.

GENERAL FEATURES OF COMPRESSIVE BUCKLING

Nonuniform, laminated elastomeric columns with curved layers in general have S-shaped first compressive buckling modes. In the case of a column which is symmetric about its center point,

†Third cycle to 25% shear strain.

Table 2. Summary of test column data and calculated critical loads

Sample No.	Spherical shim radius (in.)	Shim thickness (in.)	Column height (in.)	Layer thickness (in.)	K_B (in^2 lb)	K_S (lb)	K_{12}† (in lb)	$1-\frac{K_{12}^2}{K_B K_S}$	Observed first cycle limit load (lb)	Calculated P_c (discrete analysis) (lb)	Calculated P_c (continuum analysis) (lb)
1	(Flat)	0·035	4·317	0·144	8216·7	700·7	0	1·0000	4050	3172·2	3159·6
2	5·48	0·035	4·436	0·148	8401·4	991·8	1532·9	0·7180	3280	3016·3	3003·7
3	3·53	0·034	4·477	0·149	8417·8	1382·8	2384·0	0·5117	3250	2815·3	2803·0
4	2·05	0·031	4·903	0·163	8864·6	2842·3	4320·6	0·2591	3125	2159·3	2148·3
5	1·55	0·031	5·014	0·167	8669·7	4310·3	5585·1	0·1653	2175	1641·4	1632·0

†The K_{12} values are listed as positive values to correspond to the upward concavity of the shims in Fig. 9. The three stiffnesses were calculated by means of an approximate three-dimensional stress [7].

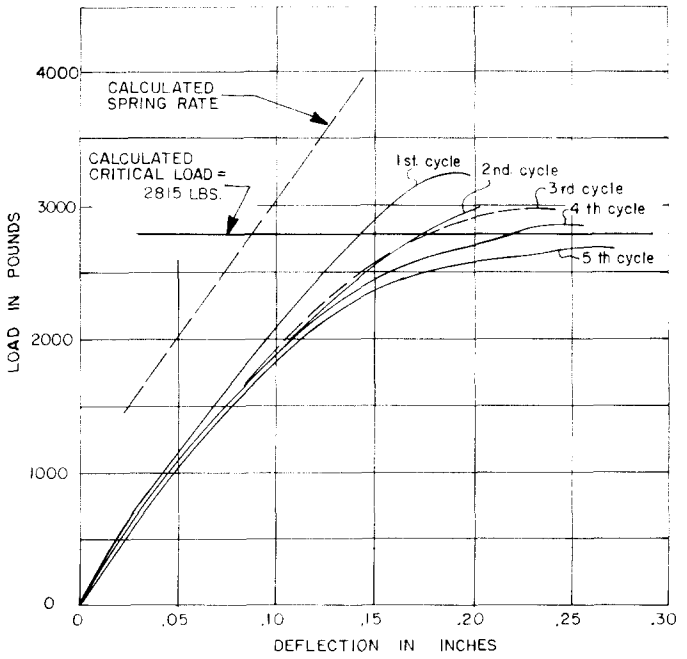

Fig. 8. Load vs deflection for sample No. 3.

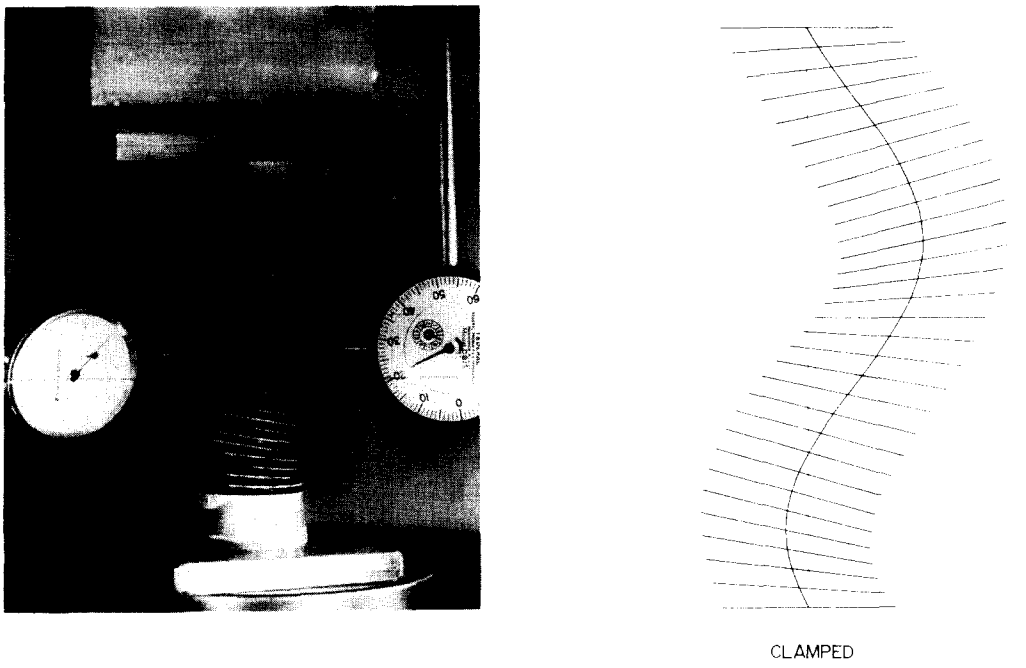

Fig. 9. Observed and calculated first buckling modes for sample No. 4.

such as test sample No. 1, this S-shape degenerates into the familiar symmetric sinusoidal first mode shape of classical elastic stability analysis. As the asymmetry of the column becomes more pronounced, so does the S-shape.

Although not shown here, the first mode shape of a tapered column having either flat or curved layers involves a large transverse displacement of the column axis near the small end and a smaller opposite displacement near the large end. The second mode shape shows the opposite behavior, that is a large excursion of the large end and a small excursion of the small end. For columns which are almost symmetric about their centers, i.e. are only slightly tapered or have nearly flat layers, the

first and second critical loads nearly coincide. For the discrete analysis, the critical load of the symmetric column is actually a degenerate double root of $\det[A] = 0$. We had initially used a bisect method to find the critical loads, but found it to fail in the case of symmetric columns for this reason. The Newton–Raphson method does not suffer this difficulty.

CONCLUSIONS

Equations were derived for predicting the effect of axial load on elastic laminated columns. They can be used to predict critical loads and mode shapes as well as the effect of sub-critical axial loads on transverse column stiffness.

Explicit results were obtained for critical solutions to columns consisting of both infinite and finite numbers of elements or layers. It was found that the finite shear stiffness and element curvature have a pronounced effect on critical loads, and in many cases produce mode shapes which are not nearly as simple as those obtained from classical buckling theory. Instability under axial tensile loads, as well as compressive loads, was shown to exist.

A comparison of continuum and discrete solutions indicated that the continuum approximation is quite reasonable provided that there are at least ten layers in a clamped column, or five layers in a pinned column. A comparison of theoretical and experimental results showed good agreement.

It should be emphasized that the analysis is based on the assumption of rigid shims, and this condition was essentially satisfied by the columns used in the experimental study described herein. However, in some applications the shims are quite thin, and the actual compressive buckling load has been underpredicted by as much as 13% because the shim deformations were significant[10].

Finally, it is of interest to observe that the shape of the lowest order tensile mode for pinned–ended columns is similar to that reported by Biot[11] for anisotropic plates under tension.

REFERENCES

1. A. N. Gent and P. B. Lindley, The compression of bonded rubber blocks. *Proc. Instn. Mech. Engrs.* **173**, 111 (1959).
2. A. N. Gent, Elastic stability of rubber compression springs. *J. Mech. Engrg. Sci.* **6**, 318 (1964).
3. J. A. Haringx, On highly compressible helical springs and rubber rods, and their application for vibration-free mountings—I. *Philips Res. Rep.* **3**, 401 (1948).
4. J. A. Haringx, On highly compressible helical springs and rubber rods, and their application for vibration-free mountings—II. *Philips Res. Rep.* **4**, 49 (1949).
5. J. A. Haringx, On highly compressible helical springs and rubber rods, and their application for vibration-free mountings—III. *Philips Res. Rep.* **4**, 206 (1949).
6. Y. C. Fung, *Fundamentals of Solid Mechanics.* Prentice-Hall, Engelwood Cliffs, New Jersey (1965).
7. R. A. Schapery, Stress analysis and thermal shrinkage of spherical HCL bearings. *Lord Library Report*, To be published.
8. R. V. Southwell, *An Introduction to the Theory of Elasticity for Engineers and Physicists*, (2nd Edn.). Oxford University Press (1941).
9. P. B. Lindley, Engineering design with natural rubber. *NRPRA Technical Bulletin* (1966).
10. D. P. Skala, Stability of elastomeric bearings, *Lord Library Report.* To be published.
11. M. A. Biot, *Mechanics of Incremental Deformations*, p. 233. Wiley, New York (1965).